ISPRS Journal of Photogrammetry and Remote Sensing 168 (2020) 28–40

Contents lists available at ScienceDirect

ISPRS Journal of Photogrammetry and Remote Sensing

journal homepage: www.elsevier.com/locate/isprsjprs

Influence of ULS acquisition characteristics on tree stem parameter estimation

Moritz Bruggisser *, Markus Hollaus, Johannes Otepka, Norbert Pfeifer

Research Group Photogrammetry, Department of Geodesy and Geoinformation, TU Wien, Wiedner Hauptstrasse 8, 1040 Vienna, Austria

ARTICLE INFO

Keywords:
Unmanned aerial vehicle
DBH
Stem diameter
Stem reconstruction
Forest inventory
Point cloud quality

ABSTRACT

We present an approach for automatically detecting the positions of tree trunks, for determining their corresponding diameter at breast height (DBH), and for assessing the shape of tree trunks from 3D point clouds derived from unmanned aerial vehicle borne laser scanning (ULS). The experiments are carried out with point clouds from both a RIEGL miniVUX-1DL and from a RIEGL VUX-1UAV. The results reveal that the autonomous stem detection recognizes 91.0% and 77.6% of the stems, respectively, and that the DBH can be modeled with biases of 2.86 cm and 0.95 cm for 80.6% and 61.2% of the trees, when compared to field measurements. We further demonstrate that, compared to terrestrial laser scanning (TLS) data, the stem diameters along the tree can be estimated with biases below 3.4 cm and 1.4 cm for the two systems, respectively, up to a tree height of 12 m for stems with a DBH above 20 cm. Our experiments further reveal the accuracy of diameter estimations to be mainly dominated by the tree's diameter with better accuracies for larger stems, while the completeness, with which a stem is covered by points, has little influence, as long as half of the stem circumference is captured. The absolute point count on the stem does not impact the estimation accuracy of all stem parameters, but is critical to the completeness with which a scene can be reconstructed. Conversely, we demonstrate the precision of the laser scanner to be a key factor for the accuracy of the stem diameter estimations, as in our experiments, we found the accuracies of the estimations from the VUX-1UAV to be higher than the ones from the miniVUX-1DL. The findings of our study assist to evaluate the potential of ULS for forest monitoring and management and allow for conclusions regarding the required point cloud qualities and, thus, the mission planning of ULS acquisitions, in order to deliver data products, which fulfill the requirements for an operational application in forest inventories.

1. Introduction

Forest inventories (FIs) aim at the acquisition of forest survey data in order to monitor the state and changes of the forests on management or country wide scales (McRoberts and Tomppo, 2007). Accurate survey data on single tree level thereby forms the basis of FIs, as single trees represent the basic entity for plot-level measurements (Saarinen et al., 2017).

The tree stem, in this context, has a vital role for biomass estimations, as it stores a substantial portion of a single tree's biomass (Muukkonen, 2006; Yu et al., 2013). Furthermore, the stem, as being the main merchantable good, is of major importance for the timber production industry, whereby stem metrics are incorporated in forest growth models (Vauhkonen et al., 2014). Finally, tree stem metrics serve as indicators of the wood quality (Van Leeuwen et al., 2011).

The biomass of a single tree can be deduced from allometric models, which take in general the stem diameter at breast height (DBH), the tree species and the tree height as input variables (e.g., Keith et al., 2000; Jenkins et al., 2003). Traditional field inventories rely on manual measurements of DBH using hand-held tools such as a caliper. This allows accurate estimates of DBH growth in multi-temporal FIs. Yet, field inventories are time-consuming (Liang et al., 2016; Piermattei et al., 2019) and the available allometric models do not consider the local characteristics of trees due to e.g., growth conditions. Furthermore, they neither comprise the measurement of the taper function, which describes the stem diameter as function of tree height, and which is used to derive the stem volume and to estimate the wood quality (Liang et al., 2014; Saarinen et al., 2017). Terrestrial laser scanning (TLS) represents a promising alternative to such field inventories, as it provides a three-dimensional representation of the forest scene in a fast and accurate way, and in millimeter-resolution. This, again, allows for the derivation of single tree parameters at plot level with accuracies

* Corresponding author.
E-mail address: moritz.bruggisser@geo.tuwien.ac.at (M. Bruggisser).

https://doi.org/10.1016/j.isprsjprs.2020.08.002
Received 26 February 2020; Received in revised form 15 June 2020; Accepted 4 August 2020
Available online 10 August 2020

comparable to field measurements, and in a reproducible way (Liang et al., 2016, 2018; Piermattei et al., 2019).

In the last two decades, several algorithms to extract tree information from TLS point clouds have been developed. Pfeifer and Winterhalder (2004), Thies et al. (2004) and Maas et al. (2008) demonstrated the feasibility to reconstruct the stems from TLS point clouds using cylinder elements, which were fitted to the stem points, and their approaches have been further automated and refined ever since (e.g., Liang et al., 2012, 2014), also addressing the reconstruction of non-circular stem-cross sections (Wang et al., 2017), and tackling the automated delineation of wood and leaf points, which is a prerequisite for proper stem modeling (Wang et al., 2016a, 2019). A comprehensive overview of available algorithms is given in Liang et al. (2018).

The accuracies of the derived stem diameter estimates were found to meet the accuracies required for FIs (Liang et al., 2016, 2018). The presented approaches further allowed the derivation of additional stem metrics such as the stem curve, which describes the diameter at any height of the stem, and, deduced from it, the stem volume.

For tree reconstructions beyond the stem, Raumonen et al. (2013) and Hackenberg et al. (2015) proposed quantitative structure models (QSMs), which use geometrical primitives for the modeling of the entire tree architecture including branches and twigs. Such QSMs allow for the estimation of the biomass of single trees up to plot level (Calders et al., 2015, 2018).

Apart from those purely data-driven approaches, models have been proposed which incorporate assumptions on tree growth or light availability for the reconstruction of the tree architecture, including the foliage (Côté et al., 2009, 2011; Bremer et al., 2017, 2018). The advantage of these approaches, despite their high computational effort, is that they can handle shortcomings in data quality, such as the typical TLS problems of occlusions and wind. Such models are of value for studies aiming at canopy structure descriptions (Côté et al., 2009, 2011) or the incorporation in sensor simulation frameworks (Bremer et al., 2017), but also allow for tree volume estimations (Bremer et al., 2018).

Yet, TLS is labour intensive and therefore expensive (Wilkes et al., 2017; Brede et al., 2019), which limits its general application for the acquisition of forest inventory data at plot level. With the advent of unmanned aerial vehicle (UAV) based laser scanning (ULS), we have a promising tool at disposal for the acquisition of forest structures at larger extents (Jaakkola et al., 2010; Wallace et al., 2012; Mandlburger et al., 2015). Early studies illustrated the potential to retrieve single tree parameters such as tree location and height, crown area, and crown volume from ULS data (Jaakkola et al., 2010; Wallace et al., 2012, 2014). With the advances in the platform and sensor systems, it is possible to capture the forest structure in a similar way and with a similar level of detail on stems and branches as with TLS systems (Morsdorf et al., 2017; Liang et al., 2019). The potential to retrieve the DBH from ULS point clouds has been demonstrated (Brede et al., 2017; Wieser et al., 2017), although the stem locations were manually detected in these studies. Liang et al. (2019) proved the applicability of stem reconstruction algorithms developed for TLS data on ULS datasets for the retrieval of the DBH, the stem curve and the stem volume, respectively, but reported lower accuracies of the respective parameters derived from ULS than from TLS datasets. Brede et al. (2019) reconstructed an entire forest plot with QSMs and found reliable tree volume estimations for large trees, when compared to TLS.

Despite the demonstration of the potential to reconstruct trees from ULS data, and to retrieve forest inventory parameters, Brede et al. (2019) and Liang et al. (2019) stressed that the accuracies of today's ULS systems limit the accuracies of these estimated parameters. In our study we investigate the potential of two ULS systems for the retrieval of forest inventory parameters, and particularly focus on the influence of the deployed sensor system and acquisition characteristics, respectively, on the accuracy of the deduced tree parameters. We adapt existing stem reconstruction approaches for TLS for the application with ULS data and present a framework which allows the autonomous stem reconstruction, including the stem detection. Modifications for the use of ULS data were necessary, as, despite the mentioned similarities in the achieved level of detail, the point density in ULS typically is lower than in TLS datasets and the height of the strongest occlusion effects are reversed (Morsdorf et al., 2018; Liang et al., 2019; Schneider et al., 2019).

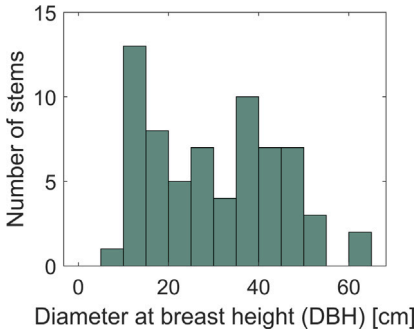

Fig. 1. DBH distribution of the 67 trees as measured in the field. Bin width is set to 5 cm.

The reconstructed forest scene allows us to devote attention to four aspects of the stem modeling from ULS data, which are:

1. the completeness of automated stem detection and the accuracy with which the DBHs of individual trees can be derived from ULS and from TLS datasets, respectively
2. the feasibility to reconstruct tree stems from ULS data, and the accuracy with which tree stem diameters can be retrieved across the tree heights, when compared to the stem models from TLS; this also includes the completeness of the reconstruction, i.e., the number of trees within the scene
3. how the point cloud quality affects the feasibility to estimate stem diameters across tree heights, and the accuracy, which can be achieved
4. the impact of the sensor's range accuracy on the accuracy of the derived stem diameters

The findings allow to draw conclusions on the potential of ULS in FIs, on the ULS sensor systems which are suitable for the retrieval of the respective parameters, and what the requirements are regarding the acquisition schemes.

2. Data

2.1. Study area

The forest scene, which we reconstructed, covers an area of 42 × 44 m^2, located in north-eastern Austria, centered at 48° 31′ 50″ N, 15° 11′ 57″ E (WGS84) and a mean elevation of around 800 m above sea level (Fig. 2). The test site is characterized by flat terrain, covered by coniferous tree species and little understory. Tree heights range from 7.9 m to 34.4 m, with DBHs in the range of 9.6 cm to 64.3 cm (Fig. 1).

2.2. Field inventory

For a total of 67 trees within the test site, a forest inventory consisting of the tree positions, DBHs, stem circumferences and tree heights was conducted. A caliper was used for the measurement of the DBHs, while tree heights were measured with a Vertex Ultrasonic hypsometer (HAGLOF INC, Madison MS, USA). We took the stem circumference as basis for the diameter references in our study. The stems were divided into three stem classes for the analysis, based on their DBH (Table 1).

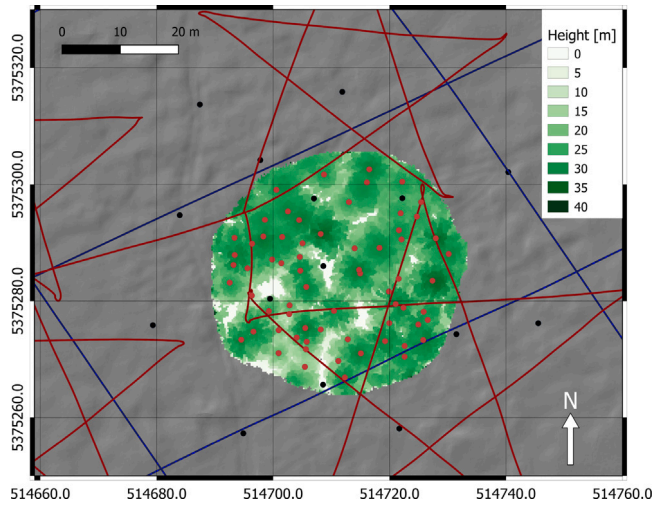

Fig. 2. CHM derived from the miniVUX data of the test site (green), with the positions of the 67 reference trees (red dots). Further depicted are the 15 TLS-scan positions (black dots), and the flight trajectories of the miniVUX (red line) and the VUX-1 (blue line), respectively. The background shows a shading of the terrain model derived from the TLS dataset (gray). (For interpretation of the references to color in this figure legend, the reader is referred to the web version of this article.)

Table 1
Number of tree stems in three stem classes.

	8 ≤ DBH < 20 cm	20 ≤ DBH < 40 cm	DBH ≥ 40 cm
Number of trees	22	26	19

Table 2
Specifications of the deployed laser scanning systems. Accuracy refers to the conformity of the range measurement with respect to the actual value and precision to the repeatability of the measurement.

Sensor	VZ-2000	miniVUX-1DL	VUX-1UAV
Field of view	+60°/−40°	23° off-nadir	330°
Scanning pattern	Hemispheric	Circular (Palmer scan)	Linear
Pulse repetition frequency	1 MHz	100 kHz	550 kHz
Wavelength	1550 nm	905 nm	1550 nm
Beam divergence	0.3 mrad	1.6 × 0.5 mrad	0.5 mrad
Footprint size @ 100 m	~ 30 mm	160 × 50 mm	50 mm
Accuracy	8 mm @ 150 m	15 mm @ 50 m	10 mm @ 150 m
Precision	5 mm @ 150 m	10 mm @ 50 m	5 mm @ 150 m

2.3. TLS data

The TLS acquisition was carried out in May 2017 using a Riegl VZ-2000 (RIEGL Laser Measurement Systems, Horn, Austria). Details on the sensor are listed in Table 2. For the data acquisition, a horizontal and a vertical beam step size of 0.2 mrad was applied, which resulted in a point spacing of 6 mm at 30 m distance from the scanner. The scene was captured from 15 scan positions, which were located in a circular shape with a diameter of 60 m around the plot, and additional scan positions within this circle in order to minimize occlusions by trees (Fig. 2). The co-registration of the scans from the 15 positions was accomplished with a standard deviation of 3.6 mm using Riegl's RiSCAN PRO software (RIEGL Laser Measurement Systems, Horn, Austria).

2.4. ULS data

Two different ULS sensor systems were deployed for the airborne data acquisition, namely a Riegl VUX-1UAV (subsequently referred to as VUX-1) and a Riegl miniVUX-1DL (referred to as miniVUX), both mounted on a RiCopter (RIEGL Laser Measurement Systems, Horn, Austria). The acquisitions were carried out on 8 November 2016 (VUX-1) and on 31 January 2018 (miniVUX), respectively.

Table 3
Pulse and point density specifications within the test site for the ULS systems.

	miniVUX-1DL		VUX-1UAV	
	Mean	Median	Mean	Median
Point density [pts/m^2]	5716.0	4973.5	1831.1	1406.5
Pulse density [pulses/m^2]	4044.4	3382	1402.0	1057.5

The flight path for the VUX-1 followed a regular criss-cross scheme (blue trajectory in Fig. 2) at a mean flight altitude of around 70 m above the terrain. During the flight mission, a larger area around the test site was covered with a total of 18 flight strips, of which the test area was present in five. The flight lines had a spacing of 80 m and 40 m in west-east and in north-south direction, respectively.

For the miniVUX, an alternative trajectory configuration was applied, consisting of a pentagram-shaped flight pattern (red trajectory in Fig. 2). The mean flight altitude for this mission was 65 m above the terrain, with the centers of the neighboring pentagrams being between 40 m and 70 m from one another.

An overview of the sensor specifications with relevance for our study is given in Table 2, while the pulse densities of the two flight missions as well as the resulting point densities are reported in Table 3.

3. Methods

3.1. Stem reconstruction from ULS

The stem reconstruction consists of four sequential steps, comprising of the identification of the stem locations (*Steps 1* and *2* in Fig. 3), the estimation of the DBH (*Step 3*) and the modeling of each tree trunk from the bottom to the top through a stem tracing scheme (*Step 4*).

Previous studies, which estimated the DBH from ULS data, used field-measured stem locations (Wieser et al., 2017) or manual inspection of the point cloud (Brede et al., 2017). However, we intended to implement an autonomous stem detection. The initial detection of the stem locations thereby was crucial for the retrieval of the DBH and the stem curve in our approach, as the entire subsequent stem reconstruction procedure based on these initially detected positions.

A number of studies have discussed the autonomous stem location detection for TLS point clouds. The proposed approaches considered the local point densities within a certain height range (Olofsson et al., 2014), the local point distribution around each point, represented by the normal vectors and the eigenvalues in the neighborhood of each point (Liang et al., 2012, 2014), or a combination of these two (Wang et al., 2016a,b). An alternative to point based methods was presented by Heinzel and Huber (2017), who performed 3D morphological operations on voxelized point clouds.

However, the acquisition characteristics and the point cloud quality between ULS and TLS differ fundamentally in three aspects. First, the point densities in TLS datasets commonly are higher (Brede et al., 2017). Second, the point density on a spot on the ground in the ULS point cloud is primarily defined by the flight lines of the UAV (Brede et al., 2017) contrary to TLS, for which the local point density is a function of the distance to the scanner (Liang et al., 2012). Third, occlusions in ULS acquisitions increase with increasing penetration depth into the canopy (Morsdorf et al., 2018; Bruggisser et al., 2019). As consequence of these three factors, we found the stem coverages within our ULS point clouds to be less uniformly distributed both across the stem heights, but also on different tree stems within the test site, when compared to the TLS dataset.

In order to cope with the given differences in the point cloud qualities, and in order to facilitate a fast computation, we pursued two concepts with our algorithm: First, we were seeking an approach that completely dispenses with normal vectors, which is reflected in *Steps 1* and *3*, respectively, of the stem reconstruction; second, we intended to

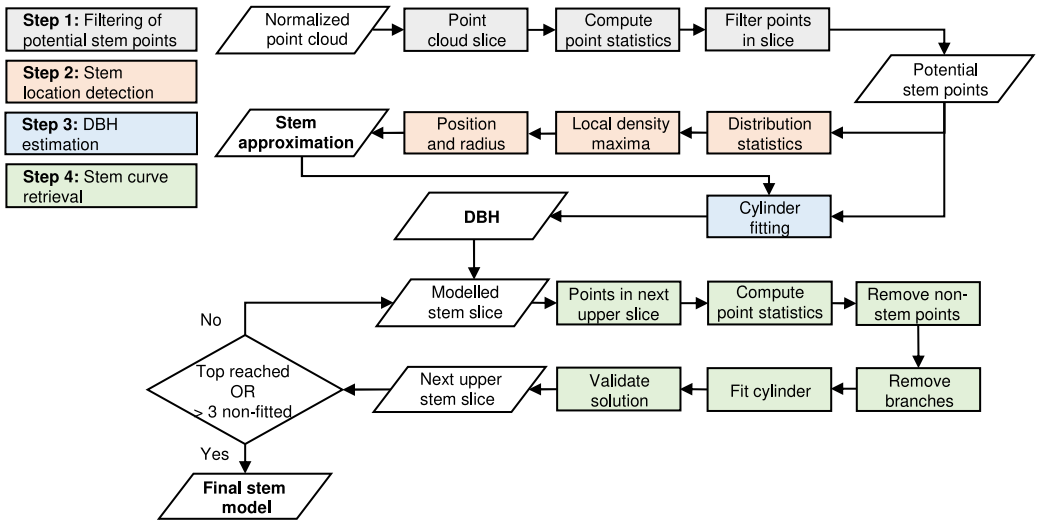

Fig. 3. Processing work-flow for the autonomous stem detection and DBH retrieval. The main products that were evaluated in the experiment are written in bold.

avoid a strict classification of the point cloud into wood and leaf points (*Steps 2* and *4*, respectively).

The workflow was built around the OPALS software package (Pfeifer et al., 2014) in order to facilitate a fast computation, which can be scaled to larger extents.

3.1.1. Step 1: Filtering of potential stem points

The basis of the entire computation consisted of a normalized point cloud, whereby the digital terrain model (DTM) was computed from the respective ULS datasets in a hierarchical approach following Pfeifer and Mandlburger (2017).

In *Step 1*, non-stem points were filtered out, only considering points in a height slice between 0.4 and 3.2 m above the terrain. While Liang et al. (2012) performed the stem detection within the entire point cloud, Olofsson et al. (2014) used a slice of 1 m height, what lowers the computation cost. However, we considered the latter height slice to be too small for the less dense ULS point clouds, why we adapted it to our data.

The idea is that stem points are characterized by a higher local point density than non-stem points. We therefore computed two point statistics describing the neighborhood around each point, consisting of the point counts (number of points) and the average point distance, which corresponds to the mean distance of the edges of the Delaunay triangulation of the point cloud in 2D. These two statistical metrics were computed for cylindrical neighborhoods of 20 cm radius around each point. However, in order to detect and subsequently remove large branches, which have similar characteristics as stem points regarding local point densities, we split the point selection into two subsets: first, only points within the search cylinder in the lower half of the height slice were considered, whereas in a second round, only points in the upper half were considered. Yet, the two metrics were computed for all points within the slice in both iterations, and the two statistical metrics for each, the lower and the upper half of the search cylinder, were attributed to each point. Finally, only points with a minimum of 1 point within the upper and the lower half of the cylinder, and with point distances < 0.1 m were retained as potential stem points.

3.1.2. Step 2: Autonomous stem location detection

The goal of *Step 2* is to identify the stem positions and to estimate the respective stem radii within the filtered slice of potential stem points in order to obtain the initial parameters for the cylinder fitting in *Step 3*. We first computed the median of the point distributions in x- and y-direction based on a cylindrical neighborhood with 0.5 m radius around each point from the filtered point cloud from *Step 1*. Median points with vertical point distributions (z-range) exceeding 1.5 m within this search cylinder subsequently were transformed into a raster with a cell size of 10 cm (Fig. 4). The z-range threshold thereby allowed to filter out dense understory, whose extent in z-range within the search cylinder was lower, while the neighborhood for the median computation was chosen in accordance to the maximum stem diameter, which we expected to be below 1 m. The 10 cm raster size, finally, generalizes the median positions of the horizontal point distributions, which coincide more frequently in the actual stem center. The grid size of 10 cm represents a trade-off between the resolution of the estimate of the stem center (higher for smaller grid sizes) and the frequency with which the median values coincide within a cell (higher for coarser grid sizes).

Within the 10 cm raster with the median locations, we computed the number of points falling into each cell and applied a local maximum filter with a search window size of 1 m. The x- and y-coordinates of the local point count maxima were retained as tree locations. Here again, the size of the neighborhood had a physical meaning, as we expected trees to stand at least 1 m apart from each other.

The radius, finally, was set to the 75%-quantile of the distances between the detected stem locations and all potential stem points within a cylindrical neighborhood of radius 0.6 m.

3.1.3. Step 3: DBH retrieval

Various approaches to retrieve the diameter from the point cloud exist. Olofsson et al. (2014) and Saarinen et al. (2017) demonstrated circle fitting to be feasible for TLS-point clouds, while Brede et al. (2017) transferred this approach to ULS data. Wang et al. (2017) used Fourier series to reconstruct the perimeter of stems from TLS data, which allows the stem cross section to be non-circular. However, due to occlusions in the ULS dataset, which resulted in some stems to be only partly captured, we decided to fit 3D-cylinders to a vertical subset of the point cloud. Such a proceeding also was chosen by Liang et al. (2012, 2014) and by Wang et al. (2016a) for point clouds from TLS and by Wieser et al. (2017) for ULS data. We expected the results to be more robust in case of only partially recorded stems slices.

The actual cylinder fitting was performed through robust least squares. The advantage of the approach lies in its ability to detect and remove point outliers during the iterations and the final adjustment.

In the fitting process, the position, orientation and radius of a cylinder for the designated stem points from *Step 1* are sought. The estimated stem locations and radii as found in *Step 2* were taken as initial parameters, and the fitting was performed for a point cloud slice of 1.8 m height. For the retrieval of the DBH, the height of the

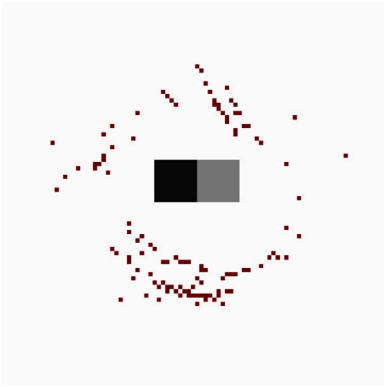

Fig. 4. Illustration of the stem location detection. The red points represent a subset of the point cloud slice between 0.4 m and 3.2 m, acquired by the VUX-1, after filtering of potential stem points (*Step 1*). For each of the 121 points present in the stem slice, the median values in *x*- and *y*-direction of the point distributions within a cylindrical neighborhood with 0.5 m radius were computed and transformed into a 10 cm raster grid. The number of points with a median position falling into a respective cell were counted and assigned to the cells (black cell: 118 points, gray cell: 3 points). After applying the local maximum filtering on the median raster, a tree position of 5375295.48 N, 514702.61 E was estimated and taken as approximation of the stem location for the cylinder fitting.

Table 4
Criteria for keeping a cylinder fitted to the stem points in *Step 3*, as valid solution. $axis_X$, $axis_Y$, $axis_Z$ correspond to the x-, y-, and z-component of the axis of the fitted cylinder, Δ R to the discrepancy between the approximated radius from the point distributions and the radius from the cylinder fitting, and *residual* to the radial standard deviation of the points to the cylinder.

Criterion	TLS	miniVUX	VUX1
min. DBH [cm]		20	
max. DBH [cm]		100	
$axis_X$		<0.3	
$axis_Y$		<0.3	
$axis_Z$		>0.9	
max. Δ R [m]		0.14	
max. residual [m]	0.014	0.05	0.036

cylinder was centered at 1.3 m above the terrain. The height of the point cloud slice, to which cylinders are fitted, was found through prior experiments. The comparison of the success-rates of the cylinder fitting and the accuracies of the estimated stem diameters to field measurements revealed a trade-off between the completeness of stem reconstruction and the accuracy of the diameter estimation, as more stems could be modeled if the slice height was extended, while the errors of the estimated diameters to the field reference were smaller for smaller height ranges. The applied height of 1.8 m turned out to be a good compromise and is in accordance to the height which was used in Wieser et al. (2017).

Finally, the fitted cylinders were accepted if they fulfilled certain criteria (Table 4) and were rejected otherwise.

3.1.4. Step 4: Stem modeling

Starting from the successfully modeled stem trunk at breast height, each tree trunk was modeled individually with cylinders through a stem tracing process along the stem axis towards the tree top. The stem diameters were estimated from the planes at the vertical center of the cylinders, whereby the height spacings between subsequent vertical centers were set to 0.5 m. During the stem tracing, a point cloud slice with a height of 1.8 m and centered at the height of the next upper stem diameter was extracted from the point cloud. From this point cloud slice, stem points were filtered based on two criteria: First, we evaluated the local point density, which we measured as the number of points and the mean point distance to neighbors (Fig. 5, left), respectively, within a cylindrical neighborhood with a radius of 20 cm around each point. Second, as we expected the stem points in the next upper stem slice to be in the horizontal proximity of the preceding stem center, we measured the distance of each point in the instantaneous slice to the axis of the preceding cylinder. Only points with a minimum point count of 3, a mean point distance < 0.029 m, and a maximum distance to the stem axis < 1.5 times the radius of the previous cylinder were retained. As in the stem filtering in *Step 2*, the remaining point cloud still included points from large branches. We therefore computed the vertical distribution of the points within a cylindrical neighborhood of 30 cm radius around each point (Fig. 5, middle) and removed points with a vertical point spread below 0.75 m. Identical to *Step 3*, we then fitted a cylinder to the filtered point cloud slice, whereby the median of the horizontal point distribution was chosen as cylinder location and the radius of the previously fitted cylinder as radius for the approximation of the current fit. In a final step, the parameters of the fitted cylinder were validated and only cylinders were retained, whose diameter and axis direction were comparable to the cylinder immediately below, and furthermore fulfilled the criteria listed in Table 4 (Fig. 5, right). This processing step was continued as long as potential stem points in an next upper stem slice were available and retained after the two filtering steps. However, as it is possible that certain stem parts are occluded for the scanner, we allowed the model to skip three consecutive stem slices, but ultimately terminated the process if none of these slices contained any stem points. The visual inspection showed that in lower stem sections at most one slice is skipped, mainly because individual stem sections were occluded. In contrast, point cloud slices from upper stem sections contain more points of leaves, which makes the recognition of the stem unreliable. The fitted cylinders therefore violate the criteria from Table 4 why the maximum of three skips are no limitation here neither.

3.2. TLS data processing

The stem reconstruction from the TLS dataset followed the same four general steps as described for the ULS datasets (Fig. 3). However, we made some adaptations in order to meet the differences in the point cloud qualities between the two data sources, which predominantly concerned the higher point density of the TLS dataset. Such modifications were necessary for performance reasons, because, opposed to Kankare et al. (2016), Puttonen et al. (2013) and Wang et al. (2016a), we did not downsample the TLS point cloud prior to the processing.

The first modification concerned the filtering of potential stem points within a point cloud slice between 1.0 m and 2.6 m above terrain (*Step 1*), which we did purely raster-based for the TLS dataset. Again, we assumed stems to be characterized by higher local point densities, opposed to non-fiber points, and by a larger spreading in vertical direction, opposed to branches. For each cell of size 10 cm, we computed the number of points, the 10%-, 50%- and the 90%-quantiles of point heights, and the point distribution in vertical direction (z-range), only selecting points between 1.1 m and 1.5 m above ground. From the computed number of points within each cell, we further computed the median and the sum of points within a circular neighborhood of 50 cm radius around each cell. These local point distribution descriptors subsequently were used to filter potential stem points from the original TLS point cloud, whereby we only retained points from cells containing more than 30 points, had a z-range larger 30 cm, spacings larger 10 cm between the 10%- and 50%-quantile, 10%- and 90%-quantile, and the 50%- and 90%-quantile, respectively, and containing more than 1000 points and a median equal to or larger 30 points, respectively, in the enlarged neighborhood of 50 cm radius.

The approximations for the stem locations and the radii, respectively, for the cylinder fitting were retrieved in the same way as for the ULS datasets (*Step 2*). The higher point density compared to ULS, however, allowed us to reduce the height of the point slice, to which the cylinder was fitted, to 0.6 m (*Step 3*).

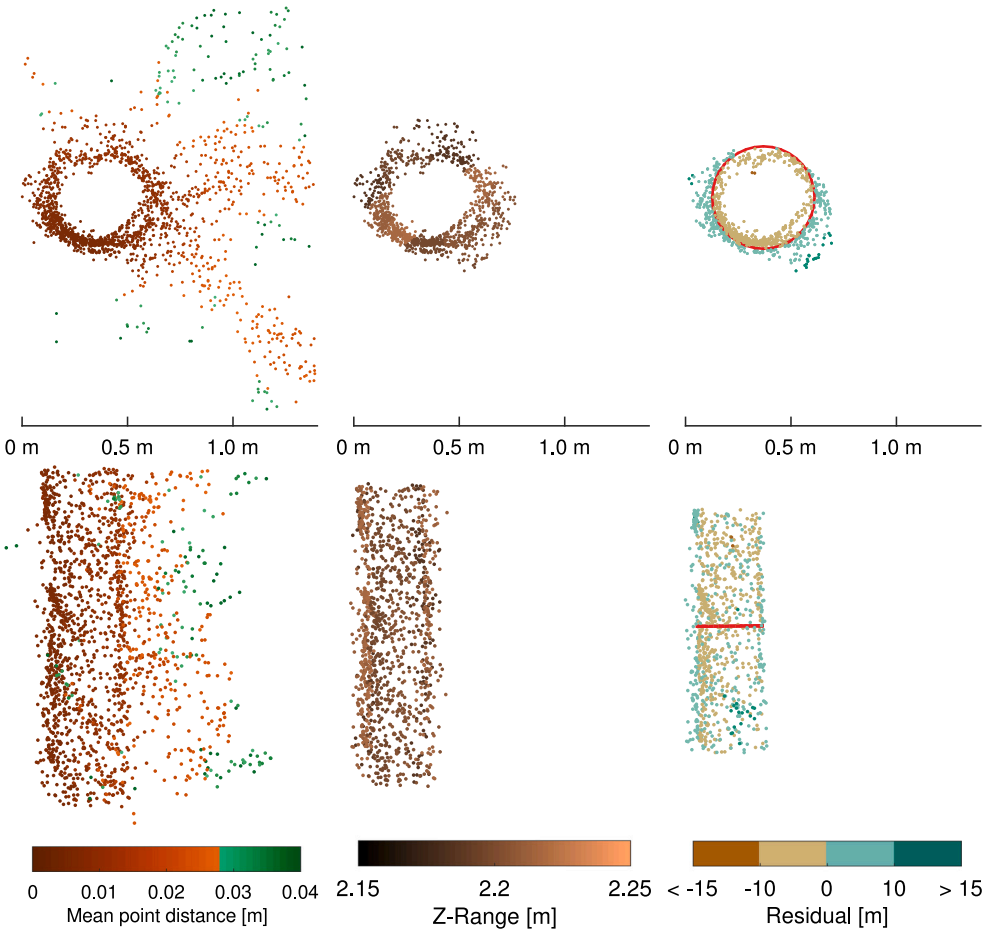

Fig. 5. Example of the filtering of non-stem points and the cylinder fitting, respectively, during the stem tracing (*Step 4*), illustrated for a point cloud subset taken from the miniVUX dataset and centered at 4.8 m above ground. Left: The unfiltered point cloud in the initial subset of the next upper stem slice, which also comprises non-stem points. The points are colored according to the mean point distance. Points with mean point distances < 0.029 m, which are accepted as potential stem points, are colored in brown, while points with larger mean point distances are colored in green. Middle: The subset after filtering based on the point count, the point distance to neighbors and the distance to the axis criteria, colored according to the vertical point distribution within the neighborhood of each point. Right: The point cloud after filtering of non-stem points, colored according to their distance to the fitted cylinder (red circle). (For interpretation of the references to color in this figure legend, the reader is referred to the web version of this article.)

The stem growing in *Step 4*, finally, was also slightly adapted. First, the height of the slice with potential stem points in the next upper point cloud slice was reduced to 1 m. Second, we computed the point count and the point distribution in z-direction on raster basis with cell sizes of 7 cm, in order to substitute the computation intense point neighborhood search. With this modifications, we could transfer the criteria for local point densities and vertical point spreadings, respectively, from ULS to TLS point clouds. Only points from raster cells with minimum counts of 15 points and a vertical spreading larger 0.6 m were retained as stem points.

The residual threshold applied for the validation of the cylinder fitting was also adjusted to the TLS point cloud (Table 4).

3.3. Experiments

All trees within the area of the field inventory plot were reconstructed from the TLS and ULS point clouds (Fig. 6). Based on these modeled stems, we tested the performance of the autonomous stem reconstruction framework and the accuracies of the stem diameter estimations in dependence of the acquisition and sensor characteristics based on four aspects (*RQ1* through *RQ4*), which we considered to be good quality measures and which also shaded light on the potential of ULS sensor systems in the context of FIs.

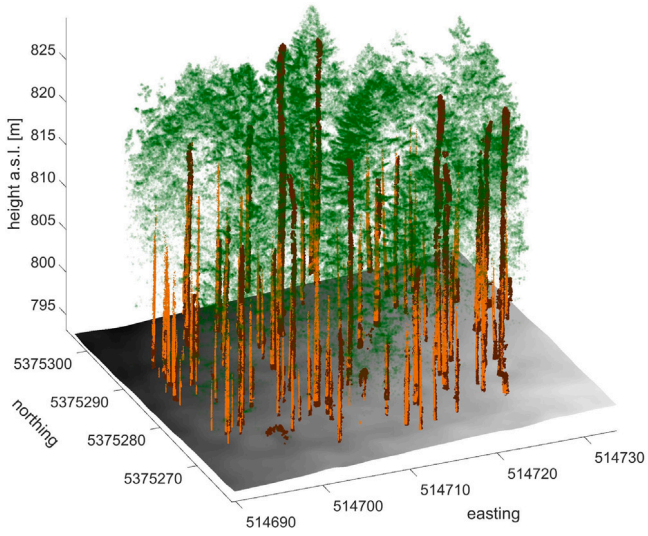

Fig. 6. Reconstructed tree stems from miniVUX (dark brown) and TLS (light brown) within the study area. A subsampling of leaf points from the miniVUX dataset is shaded in green. (For interpretation of the references to color in this figure legend, the reader is referred to the web version of this article.)

3.3.1. Autonomous stem detection and DBH retrieval (RQ1)

Each detected stem location from the point clouds was compared to the stems in the field inventory and a detected stem was accepted as correct if its position was within a 0.5 m distance from an actual stem. These stems correspond to true positives (*TP*). We then computed the precision and the recall to evaluate the performance of the autonomous stem detection:

$$precision = \frac{TP}{TP + FP} \tag{1}$$

$$recall = \frac{TP}{TP + FN} \tag{2}$$

where *FP* corresponds to point cloud clusters which were recognized as stems by our algorithm but were not reported in the field inventory (false positives), and *FN* to stems in the field inventory, which were not detected in the point cloud (false negatives).

The DBHs estimated from the point clouds were compared to the measurements form the field inventory. The number of estimated DBHs, which were retained after filtering of invalid solutions and which could be matched to the field inventory, was counted and the accuracy of the estimated DBH measured in terms of the *bias* and the *RMSE*:

$$bias = \frac{1}{n}\sum_{i=1}^{n}\left(DBH_{ls,i} - DBH_{ref,i}\right) \tag{3}$$

$$RMSE = \sqrt{\frac{\sum_{i=1}^{n}\left(DBH_{ls,i} - DBH_{ref,i}\right)^2}{n}} \tag{4}$$

$DBH_{ls,i}$ thereby corresponds to the ith DBH estimation from the point cloud, $DBH_{ref,i}$ to the respective measurement from the field inventory, and n to the number matched DBHs.

3.3.2. Stem reconstruction (RQ2)

We used the stem diameters across the tree heights as retrieved from TLS through our processing chain as reference to which we compared the stem diameter estimates from the two ULS point clouds. Each reconstructed tree stem from the ULS data was connected to a stem derived from the TLS data, again applying a 0.5 m maximum horizontal displacement threshold for the match. We computed the difference between the retrieved diameters across the stem height and evaluated the completeness with which the scene at each height could be reconstructed.

3.3.3. Effect of the point cloud quality (RQ3) and sensor characteristics (RQ4)

We analyzed how the number of points within a stem slice, and the completeness with which a stem circumference was covered by points, respectively, affected the accuracy of the estimated stem diameter (*RQ3*). To measure the coverage of the stem circumference, the stem points were projected onto a horizontal plane (Fig. 7). Assuming a roughly circular stem cross section, we took the median of the point distribution of a stem point slice as circle center and split the circle into eight equal sectors with the orientation of the circular division towards north. A fraction of the stem circumference was considered as captured if the corresponding circle sector contained at least three stem points projected onto the horizontal plane.

The influence of the sensor's range precision on the diameter estimates was tested based on the distance of the stem points to the fitted cylinders, which was measured as the radial standard deviation of the points to the latter (*RQ4*).

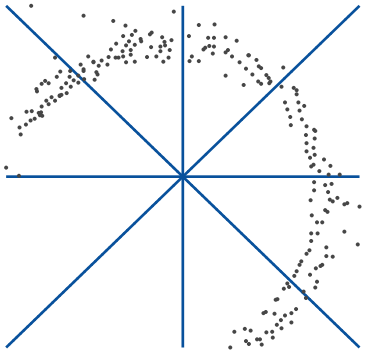

Fig. 7. Point cloud of a stem slice between 1.9 m and 3.7 m above ground from a tree stem centered at 5375291.6 N, 514708.2 E. The points were acquired by the VUX-1 and projected onto a horizontal plane (black dots). The blue lines divide the point cloud into eight equal sectors. In the example, six out the eight sectors contain points, what corresponds to a stem coverage completeness of 0.75.

Table 5
Performance of the autonomous stem detection and of the stem reconstruction for DBH estimation. *Detected trees* refers to the number of point clusters, which were regarded as stems by our detection approach, *Correctly detected trees* is the number of these clusters which could be linked to the field reference. *Valid fitted stems* corresponds to the number of *Detected trees*, for which the cylinder fitting resulted in valid solutions, *Fitted and correct stems* is the number of valid stem reconstructions which could be linked to entries in the reference.

	TLS	miniVUX	VUX-1
Detected trees	83	73	63
Correctly detected trees	65	65	55
Precision [%]	78.3	89.0	87.3
Recall [%]	97.0	97.0	82.1
Valid fitted stems	64	61	44
Fitted and correct stems	61	54	41
DBH bias [cm]	−0.34	2.86	0.95
DBH RMSE [cm]	1.92	5.26	2.63

4. Results

4.1. Autonomous stem detection and DBH retrieval (RQ1)

Table 5 reports the number of trees which were correctly detected within the TLS, the miniVUX and the VUX-1 point clouds in terms of absolute numbers, precision and recall.

The autonomous stem detection recognized 83, 73 and 63 stem positions in the point clouds from TLS, miniVUX and VUX-1, respectively, of which 65, 65 and 55 could be matched to stems in the field inventory. Precision was higher for the miniVUX (89.0%) and the VUX-1 (87.3%) datasets than for TLS (78.3%), while the recall was highest for TLS (97.0%) and the miniVUX (97.0%) and a lower value for the VUX-1 (82.1%).

After elimination of invalid solutions (Table 4), 64 (77.1% of the initially fitted cylinders), 61 (83.6%) and 44 (69.8%) DBH estimations were retained for TLS, the miniVUX and the VUX-1, respectively, of which 61 (completeness = 91.0%), 54 (completeness = 80.6%) and 41 (completeness = 61.2%) could be linked to trees in the field inventory for the respective datasets. The accuracy of the DBH estimations was highest for TLS (bias = −0.34 cm, RMSE = 1.92 cm), followed by VUX-1 (bias = 0.95 cm, RMSE = 2.63 cm) and lowest for the miniVUX (bias = 2.86 cm, RMSE = 5.26 cm) (Fig. 8).

4.2. Stem reconstruction

In our study, we took the diameter estimates from TLS as reference to which the estimates from ULS were compared. Fig. 9 shows the difference between the diameter estimates from ULS and TLS in

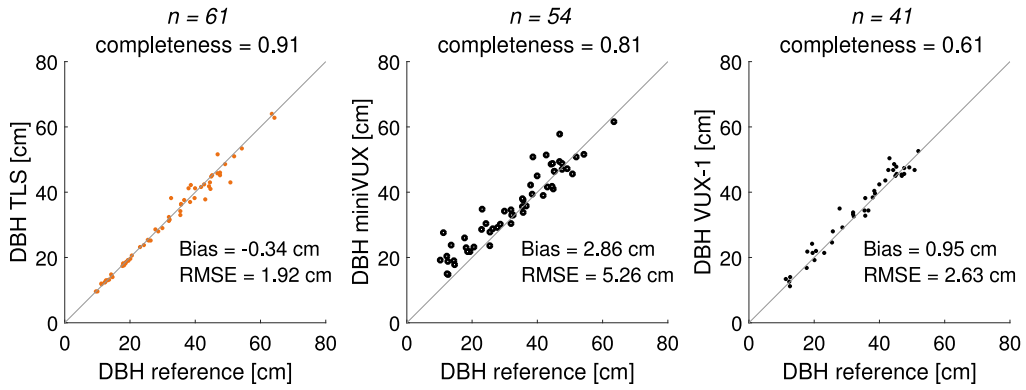

Fig. 8. Estimated DBHs from TLS (left), miniVUX (middle), and VUX-1 (right) compared to field measured DBHs. The black lines represent the 1:1 match. Further reported are the number of retrieved DBH estimates (*n*), the respective completeness with regard to the stems in the field inventory, and the bias and the RMSE of the estimations.

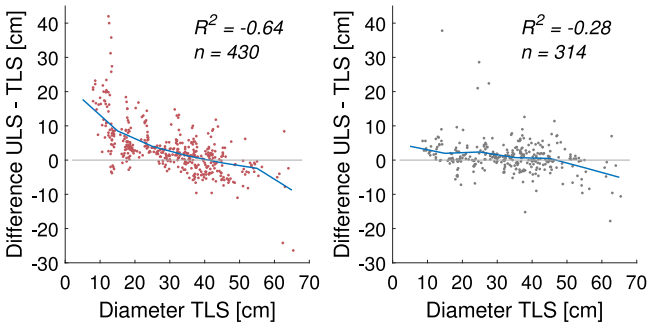

Fig. 9. Deviations to the TLS estimated stem diameters of the stem diameters estimated from the miniVUX (left) and the VUX-1 (right) dataset, respectively, in dependence of the stem diameters from TLS. Depicted are all estimated stem diameters in the range between 1.3 and 5.3 m. The blue lines depict the mean deviations between the systems in 10 cm intervals on the stem diameter axis. (For interpretation of the references to color in this figure legend, the reader is referred to the web version of this article.)

dependence of the diameter measured from TLS. Only diameters up to a height of 5.3 m were selected for this first analysis, in order to prevent a bias introduced by leaves or small branches. The absolute deviations between the systems reveal small diameters to be overestimated from the ULS datasets, particularly from the miniVUX data, however, with a decreasing trend (R^2 = −0.64 for the miniVUX, R^2 = −0.28 for the VUX-1) with increasing stem diameter sizes.

Due to this observed diameter dependency of the reconstruction accuracy, we divided the stems into three stem size classes (Table 1) to further investigate the accuracy of the diameter estimations from the ULS datasets across the tree heights. Fig. 10 depicts the mean and the standard deviations of differences between the stem diameters estimated from TLS and the miniVUX, and the VUX-1, respectively, across absolute tree heights in 1.5 m intervals, starting at breast height (1.3 m). Three subsequent diameter estimations for each stem, taken in 0.5 m intervals and centered around the evaluation heights, were summarized as their mean diameter every 1.5 m, in order to avoid gaps from missing diameter estimates due to occlusions or elimination of cylinders with invalid parameters. Depicted alongside the differences is the fraction of trees which could be reconstructed and resulted in valid solutions on each tree height.

For all three stem classes and for all tree heights, largest discrepancies in terms of the mean differences (bias) as well as the standard deviation between TLS and ULS occurred in the smallest tree stem class (DBH = 8 cm–20 cm, absolute differences between 0.5 cm–4.6 cm and 2.3 cm–10.7 cm for VUX-1 and miniVUX, respectively). Diameter differences for the larger two stem classes and up to a height of 14 m were smaller and in a comparable range for a respective sensor (absolute differences between 0.1 cm–1.6 cm and 2.3 cm–4.0 cm for VUX-1 and miniVUX, respectively, for DBH = 20 cm–40 cm; absolute differences between 0.1 cm–1.1 cm and 0.5 cm–2.4 cm for VUX-1 and miniVUX, respectively, for DBH > 40 cm). Above 14 m, the differences between TLS and ULS increased. Considering the two deployed ULS systems, we see that the differences between the VUX-1 and TLS were smaller in general than the respective differences of the miniVUX.

The fraction of trees, which could be reconstructed from bottom to top, was higher for the miniVUX than for the VUX-1 in general. Of the 24 trees with matches to TLS in the medium stem class, 45.8% could be modeled up to 10 m from the miniVUX, while in the VUX-1 data, the amount of 75% of the stems, which were initially detected, drops to 33.3% on 10 m. For the largest stem class, the rates amount to 77.8% and 66.7% of successfully reconstructed stems on 10 m for the miniVUX and the VUX-1, whereas in the VUX-1 dataset, 88.9% of the stems were initially detected.

4.3. Effect of acquisition characteristics (RQ3) and sensor properties (RQ4)

The impact of the number of points on the accuracy of the diameter estimations is depicted in Fig. 11 for 938 valid cylinders from the miniVUX (left) and for 756 cylinders from the VUX-1 (right) dataset, respectively, where the diameter differences between ULS and TLS are shown as function of the number of points within a slice. The number of points per slice after filtering of leaf- and branch-points ranged from 8 to 1145 for the miniVUX and from 6 to 294 for the VUX-1. The results show the deviation between ULS and TLS to be independent of the number of points (R^2 = −0.03 for the miniVUX, R^2 = 0.02 for the VUX-1).

The effect of the stem coverage is shown in Fig. 12, which illustrates the deviation of the estimations from the miniVUX (left) and the VUX-1 (right) datasets to the TLS diameter estimates against the completeness, with which the stem circumference was captured. 3.3% and 16.0% of the stem slices with valid cylinder fits in the miniVUX and the VUX-1 dataset, respectively, were captured with coverages smaller than half the stem circumference, while a full coverage of the stem marks the largest coverage class for both systems. The mean difference of the estimates from the miniVUX to TLS shows a decrease from 6.2 cm to 2.7 cm for coverages of 50% to 100%. For the VUX-1, the mean deviations to TLS in the respective classes are in ranges of 1.8 cm to 1.01 cm. For stem coverages below half of the stem, differences between the diameters from the miniVUX and TLS increase, but remain relatively constant for the VUX-1. However, the standard deviations for smaller coverages increase for both systems.

On the other hand, 51.5% and 69.2% of the stem slices, which could not be reconstructed with cylinders from the miniVUX and the VUX-1 datasets, respectively, were captured with completeness below half of the stem.

A final component, which interferes with all other aspects of the measurement process, is the deployed sensor itself. Our interest was

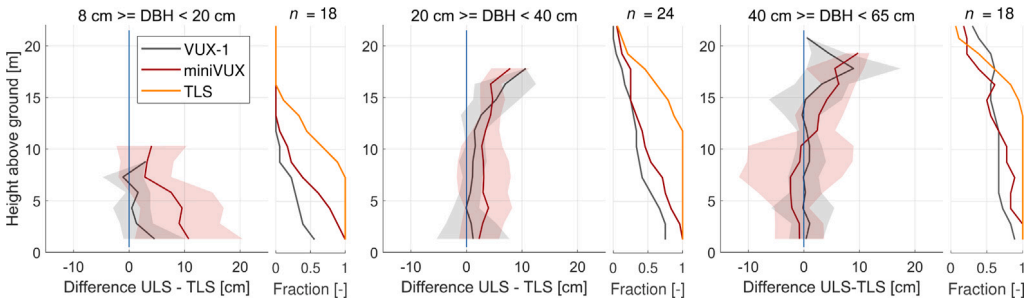

Fig. 10. Left to right: Absolute differences in the diameter estimations between ULS and TLS against absolute tree heights for stem classes 8 cm ≤ DBH < 20 cm, 20 cm ≤ DBH < 40 cm, 40 cm ≤ x < 65 cm. Also depicted is the fraction of trees, which could be reconstructed on each height. 100% thereby corresponds to the number of trees (*n*) which were detected in the TLS dataset at breast height and which could be matched to trees in the ULS datasets.

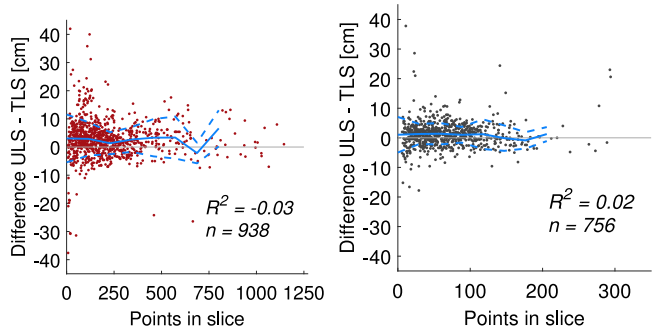

Fig. 11. Absolute difference between diameter estimations from ULS and TLS in dependence of points within a slice for the miniVUX (left) and the VUX-1 (right). Seven and two slices with relative errors larger 500% to the respective TLS estimations have been removed for the visualization from the miniVUX and the VUX-1 data, respectively. The blue solid line represents the bias to the TLS estimations, calculated in point count intervals on the *x*-axis amounting to 10% of the maximum point count for the respective system, but cut at the 97.5% quantile of the point counts, the dashed lines mark the standard deviations. (For interpretation of the references to color in this figure legend, the reader is referred to the web version of this article.)

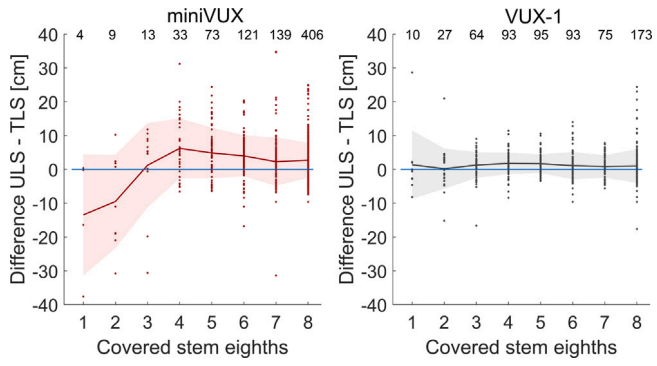

Fig. 12. Absolute diameter estimation differences between ULS and TLS to the completeness of stem coverage by points. The *x*-axis counts the stem eighths which are filled with points. The dots represent the difference values of single stem slices. The solid lines represent the bias of the ULS to the estimations from TLS per coverage class for the miniVUX (left) and the VUX-1 (right), the shaded areas represent the standard deviation of the differences. Further stated is the number of stem slices in each class (top row).

to test whether the differences in the accuracies and precisions of the two ULS sensor systems (Table 2) had an impact on the accuracy of the diameter estimations. We therefore analyzed the dispersion of the points within a stem slice around the fitted cylinder, which was measured as radial standard deviation of the points to the latter, and was summarized as residual value. We traced the progression of the residuals along the stem height (Fig. 13, left), and also related the residuals to the diameter differences between TLS and ULS (Fig. 13, middle and right).

The residuals of the points to the fitted cylinders are larger for the points from the miniVUX than from the VUX-1 and increase from bottom to the top of the stems, however, with a slightly smaller increase trend within the bottom 10 m (residuals between 3.3 cm and 3.7 cm and a mean of = 3.5 cm for the miniVUX, and between 1.4 cm 1.9 cm with a mean = 1.6 cm for the VUX-1), and a more distinct trend above (residuals between 3.5 cm and 4.9 cm for the miniVUX, and between 1.4 cm and 3.3 cm for the VUX-1).

The residuals reveal a small correlation to the differences of the estimated diameters between TLS and the miniVUX, and the VUX-1, respectively (R^2 = 13.0% and R^2 = 0.4%) within the bottom 10 m of the stem (Fig. 13, middle). However, the correlation between the diameter differences and the residuals in upper canopy parts is higher (Fig. 13, right; R^2 = 35.6% and R^2 = 31.5% for the miniVUX and the VUX-1, respectively).

The profiles in Fig. 14 show the distribution of points around the fitted cylinders for the same tree and the identical stem slice, taken from the filtered point clouds from the miniVUX and the VUX-1, and centered at 4.8 m above ground. As can be recognized, the magnitude of horizontal scattering of the points around the fitted cylinder is larger for the miniVUX (distances to the cylinder in range −11.6 cm to 15.0 cm, for 942 points) than for the VUX-1 (distances in range −3.7 cm to 9.7 cm, for 194 points).

5. Discussion

5.1. Autonomous stem detection and DBH retrieval

The identification of stem locations marks a key step within our stem reconstruction framework, as the stems subsequently are traced towards the top starting at these very positions, and is a prerequisite if forest inventories should be automated on larger extents and on an operational level. While the autonomous stem detection has been issued in several studies for TLS datasets (e.g., Liang et al., 2012; Olofsson et al., 2014; Wang et al., 2016a), stem reconstruction from ULS in previous studies predominantly relied on field measured stem positions (Wieser et al., 2017) or the manual detection of stems within the point cloud (Brede et al., 2017).

The tree detection rates we could achieve with our approach from TLS and the miniVUX (97.0% for both systems) is in the range of what was reported by other studies (Olofsson et al., 2014; Wang et al., 2016a). Yet, the detection rate was lower for the VUX-1 dataset, within which 15 stems with DBHs between 10 cm and 45 cm either were not detected or could not be linked to a tree from the field inventory. However, the visual inspection of the non-filtered VUX-1 point cloud revealed that the missed stems were not fully covered by points, neither in terms of the completeness of the stem's circumference nor in terms of a continuous and complete vertical coverage with points in the evaluated height (0.4 m–3.2 m). A locally insufficient stem sampling

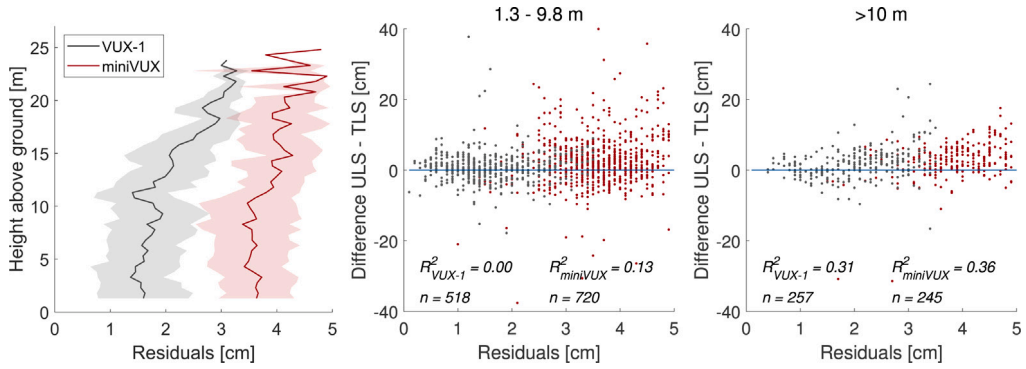

Fig. 13. Left: Mean (solid line) and standard deviation (shaded are (a) of the residuals of the stem slices along the stems reconstructed from the miniVUX (red) and the VUX-1 (black) datasets. Middle and right: deviation between the diameter estimations from miniVUX and VUX-1, respectively, to diameters from TLS as function of the residuals within a stem point slice for the bottom 10 m of the stems (middle), and for stem parts above 10 m (right). (For interpretation of the references to color in this figure legend, the reader is referred to the web version of this article.)

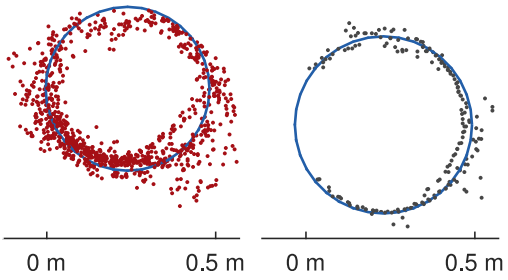

Fig. 14. Stem point profiles taken from the filtered point clouds as used for cylinder fitting, centered at 4.8 m height above ground, and taken from the miniVUX (left) and the VUX-1 (right) dataset, respectively. Both slices show the identical stem slice from a tree centered at 5375291.6 N, 514708.2 E.

has been reported for ULS data before (Liang et al., 2019) and can be attributed to occlusion effects, which for ULS were described to occur predominantly within the bottom parts of the canopy (Wieser et al., 2017; Morsdorf et al., 2018; Bruggisser et al., 2019). We therefore attribute the omission of stem locations to the less complete stem sampling that was achieved with the VUX-1 acquisition, while the denser sampling schemes of TLS and the miniVUX supported a more complete stem identification.

The DBH with our approach could be estimated with high accuracies from TLS, which are in the range of accuracies which were reported in previous studies (Lindberg et al., 2012; Wang et al., 2016a, 2017). In contrast, the accuracy of the DBH estimations from the VUX-1 data was slightly worse, in accordance to Brede et al. (2019), who applied cylinder fitting to data from the same sensor, while the accuracy for the miniVUX was lower.

The fraction of trees within the scene, for which the DBH could be estimated and was accepted as valid solution, was highest for TLS, but showed lower values for the miniVUX and the VUX-1. The elimination of DBH estimations with improbable parameters decreased the completeness of the initially retrieved DBHs by 3.1%, 6.9% and 8.9% for TLS, the miniVUX and the VUX-1, respectively, however, increased the reliability of the DBH estimations. We thereby found the deviation of the radius between the initial solution and the fitted cylinder (Δ R in Table 4) and the maximum tolerated residuals, in this order, to be the most relevant of the evaluated criteria. Yet, only stems with DBH < 40 cm were affected by these two filtering criteria.

5.2. Stem reconstruction

Previous studies demonstrated the ability to retrieve the stem tapering from TLS data with accuracies in ranges as required for the use in FIs (Liang et al., 2016, 2018; Saarinen et al., 2017) when using automated processing frameworks (e.g., Maas et al., 2008; Wang et al., 2016a; Saarinen et al., 2017). Following the experimental set up of previous studies, which aimed at the retrieval of FI parameters (e.g., Brede et al., 2019; Liang et al., 2019; Piermattei et al., 2019), we therefore took TLS as reference to which we compared the stem diameter estimates from ULS.

We found that differences between diameter estimates from TLS and ULS were smaller for larger stem diameters (Fig. 9). Stems with DBHs > 20 cm could be reconstructed from ULS with differences to TLS below 1.6 cm and 4.0 cm from the VUX-1 and the miniVUX datasets, respectively, up to a height of 14 m (Fig. 10). On tree heights above, differences between ULS and TLS increased. Increasing errors in the stem curve or volume estimation within the upper canopy, however, are a phenomenon, which was described both for TLS and for ULS (Maas et al., 2008; Wang et al., 2016a; Brede et al., 2019). Yet, if we consider a tree with a DBH of 45.2 cm and a height of 29.0 m (tree parameters taken from our field inventory), and a cone-shaped stem, the stem volume fraction, which is comprised in the bottom 10 m, amounts to 71.9% of the total stem volume. The respective volume overestimation for the bottom 10 m of the stem would amount to 7.1% for an assumed constant overestimation of the diameters of 1.6 cm (VUX-1). This implies that the fraction of the stems, which contribute the most to the stem volume, can be reconstructed from the VUX-1 with accuracies which are close to reported biases for diameter estimations from TLS (Maas et al., 2008; Liang et al., 2016).

Another aspect, however, that has to be considered alongside the diameter estimation accuracies, regards the number of tree stems, which could be reconstructed up to a certain height. The number of stems, for which diameters could be estimated up to 10 m above ground, did not show any decline within the TLS dataset, but decreased continuously for both, the miniVUX and the VUX-1, with higher fractions of reconstructed trees for the miniVUX than for the VUX-1 for all stem classes and across all heights. However, if the completeness of the stem reconstruction is considered with regard to the stems, which were detected and modeled at breast height in the respective datasets, we see that 45.8% and 77.8% (miniVUX) and 44.4% and 75.0% (VUX-1) of the initially recognized trees of the medium and the largest stem class, respectively, were reconstructed up to 10 m above ground. In that respect, the success rates of the stem reconstruction was comparable for both datasets, if a stem trunk was detected. We therefore deduce that our approach works equally well for both systems, in terms of the completeness with which a forest scene can be reconstructed, and again ascribe the lower absolute completenesses for the VUX-1 to the lower point density in this dataset.

On the other hand, the fraction of reconstructed trees dropped markedly within the upper canopy parts. Yet, the principle reproducibility of the stems towards the tree top is limited, as even for nearly

windless conditions, movements in the upper canopy parts are present and lead to a blurring of the tree structure, in particular when multiple scan lines are combined (Côté et al., 2011; Hackenberg et al., 2015).

The diameter estimates from ULS for trees with DBHs < 20 cm, finally, did not correspond well to those from TLS.

5.3. Effect of acquisition characteristics and sensor properties

In our study, we observed that the point cloud quality, consisting of the position accuracies of the points and the point density, has a major impact on the feasibility of stem reconstructions. The factors, which control the qualities of ULS point clouds, are the same system parameters as for ALS, comprising the flight altitude and speed, pulse repetition frequency, beam divergence (Hopkinson, 2007; Morsdorf et al., 2008; Næsset, 2009) and the scan angle (Morsdorf et al., 2008). However, due to the miniaturization of ULS systems, Brede et al. (2019) and Liang et al. (2019) argued that particular emphasis should be put on the sensor's range accuracy and precision, and the accuracies with which the position and the attitude of the platform can be measured.

The point cloud properties impact the derivation of stem diameters from ULS in multiple, yet different ways. We can distinguish between effects related to the point coverage on the targets, and the accuracy of the LiDAR measurements.

The impact of the first component, the point coverage on the stems, is manifested in the absolute number of points within a stem slice on the one hand, and in the fraction of the stem circumference, which is covered by points, on the other. Our results revealed the comparability of the diameter estimates between ULS and TLS to be unaffected by the absolute number of points within a stem slice, but, conversely, recognized considerably lower stem detection rates for lower point densities, as well as fractions of stems within the test site, for which the DBH retrieval and the stem reconstructions were successful. As our stem detection and reconstruction approach relies on local points densities, the higher point densities in the TLS and the miniVUX datasets were beneficial and explain the better performance compared to the VUX-1 dataset, which had lower point densities. In this sense, the weaker performance of the reconstructions from the VUX-1 dataset compared to the miniVUX is not inherent to the sensor system, but a result of the implemented scan mechanism (linear scan vs. circular scan), applied flight trajectory (criss-cross vs. pentagram-shaped) and flight altitude (70 m vs. 65 m), resulting in a sparser sampling scheme for the former sensor. However, the achieved point density is not only a function of the pulse density, but is also controlled by the penetrability of the laser beam into the canopy. This, again, is dominated by the complexity of the canopy structure, the tree species, the phaenology (Brede et al., 2019; Liang et al., 2019) and the beam divergence (Gaveau and Hill, 2003; Hopkinson, 2007; Wieser et al., 2016). Considering the better penetrability into the canopy for smaller footprint sizes as reported by Wieser et al. (2016), the smaller footprint of the VUX-1 compared to the miniVUX is favorable for forestry applications and we expect that an acquisition with a denser sampling scheme would increase the performance of the stem reconstruction from the VUX-1 dataset.

The completeness of the stem circumference, which is covered with points, is another aspect of the point coverage. We found higher correspondences in the diameter estimations between ULS and TLS if at least 50% of the stem circumferences were covered with points in the ULS dataset, but larger differences below that threshold. On the other hand, the majority of the stem slices, which could not be modeled with cylinders, revealed coverages below half of the stem circumferences. Therefore, also the completeness, with which the stem circumference was captured, impacts the success rate of the stem reconstructions, apart from the mere point count on the stem. However, we anticipate that a sufficient stem coverage with regard to both criteria can be achieved through a regular criss-cross trajectory, if the strip overlap is large enough. For the VUX-1, a distance between parallel flight lines of 40 m at a flight altitude of 70 m above ground proved to be sufficiently dense for our test site. However, the number of points on the stems also depends on the density of the canopy and a general statement is difficult to make. On the other hand, the gain from a pentagram-shaped trajectory is rather small.

The position accuracy of the points within the point cloud represents the second component impacting the point cloud quality, and was discussed to be a major limiting factor for the application of ULS systems in precision forestry (Brede et al., 2019; Liang et al., 2019). In our study, we analyzed the influence of the residuals of the stem points around the fitted cylinders on the accuracy of the diameter estimates from ULS. The impact of the residuals on the differences between a respective ULS system and TLS was small to negligible within lower, and medium within upper canopy parts. Yet, our results revealed larger residuals to the fitted cylinders in general for the miniVUX than for the VUX-1 within the bottom 10 m of the stems, which were not covered by understory or leaves and therefore had a distinct stem. We, thus, consider that the residuals can be attributed to the accuracy of the sensor system, if analyzed for such distinct structures. If we leave aside the accuracy with which the position and attitude of the platform are measured (cf. Brede et al., 2019; Liang et al., 2019), we can assume that a higher accuracy is related to a smaller footprint in general. On the one hand, the area within which a backscattering object is located is more precisely determined and therefore less uncertain for smaller footprints. At the same time, the distance measurement will be triggered by the first reflected signals. With a larger footprint size and a simultaneous oblique incidence angle of the laser on the stems, the measurement is not triggered by the stem components in the center of the footprint, but by stem parts from the upper area within the laser beam. These sections of the stem, however, are closer to the sensor under the given acquisition geometry, leading to an underestimation of the distance and, as a consequence, to an overestimation of the diameter. These two processes related to the footprint size would explain the observed decreasing accuracy with increasing footprint size from TLS to the VUX-1 and towards the miniVUX, both in terms of the system accuracy and the accuracy of the DBH estimation.

6. Conclusion

We presented a framework for the autonomous stem detection and stem reconstruction from ULS point clouds. Our approach is based on a stem tracing approach from bottom to the tree tops, whereby cylinders are fitted to the point cloud using least-squares. The functioning of our approach was tested for both, a Riegl VUX-1UAV and a Riegl miniVUX-1DL laser scanning system. The comparison of the estimated stem diameters across tree heights from the ULS systems to the field-measured diameters at breast height, and to stem diameters estimated from TLS above, respectively, revealed the accuracy of the VUX-1UAV derived estimates to be close to TLS, while the discrepancies to the references were larger for the miniVUX-1DL.

The experimental set-up further allowed to assess the impact of the point cloud qualities on the retrieved accuracies of the stem diameter estimates, in particular the point densities and the system accuracies of the sensor.

While the accuracy of the estimated stem diameters from both ULS-systems were higher for tree stems with larger diameters, we found the number of points on the stem to have no impact on the retrieved accuracy. Higher completenesses, with which the stem circumference was captured, on the other hand, increased the accuracy of the diameter estimates, while the discrepancies to the reference dropped for stem coverages below 50% of the stem circumference. The analysis of the cylinder fitting process, finally, revealed larger residuals for the miniVUX-1DL than for the VUX-1UAV. We, thus, anticipate that the higher correspondences of the diameter estimates from the latter system to the reference can be attributed to the higher accuracy of this very sensor system.

In contrast, we found the point density and the stem coverage to impact the stem detection and reconstruction rates, as for a higher coverage of the stem in both, the vertical direction and around the stem circumference, the completeness with which a stem could be reconstructed from bottom to the top was higher. For stem circumference coverages below 50%, the reconstructibility was weak.

Our findings suggest that the completeness, with which the stems within a forest scene can be detected and reconstructed, is increased, if a sufficiently high point density is achieved, and if a stem is captured from multiple directions. The success rate therefore can be increased through a thorough mission planing, whereby we anticipate a criss-cross pattern to be an optimal flight scheme, and parallel flight lines to be sufficient, given that a large enough strip overlap is ensured. In our tests, we found that the stem slices, which could be reconstructed from the VUX-1 dataset with differences < 5 cm to TLS, comprised 6 to 286 points, after points from branches and leaves have been filtered, while an acquisition pattern with spacings between parallel flight strips of 40 m at a flight altitude of 70 m was dense enough.

ULS systems allow the coverage of larger areas (typically several hectares to a few km^2) and thereby the acquisition of stem shape information for more trees than is the case in classical FIs or from TLS. In our study, we could demonstrate the feasibility to autonomously detect and model trees from ULS datasets. Based on such information from our tree reconstruction, we are able to derive locally adapted allometric models in a very time-efficient way, what would not be possible with TLS or in-situ measurements. Despite the lower accuracy of the estimated stem diameters from ULS compared to TLS and field inventory measurements, we therefore see a clear benefit in using ULS systems within FIs.

Declaration of competing interest

The authors declare that they have no known competing financial interests or personal relationships that could have appeared to influence the work reported in this paper.

Acknowledgment

The authors acknowledge the TU Wien University Library, Austria for financial support through its Open Access Funding Program.

References

Brede, B., Calders, K., Lau, A., Raumonen, P., Bartholomeus, H.M., Herold, M., Kooistra, L., 2019. Non-destructive tree volume estimation through quantitative structure modelling: Comparing uav laser scanning with terrestrial lidar. Remote Sens. Environ. 233, 111355. http://dx.doi.org/10.1016/j.rse.2019.111355.

Brede, B., Lau, A., Bartholomeus, H., Kooistra, L., 2017. Comparing RIEGL RiCOPTER UAV LiDAR derived canopy height and DBH with terrestrial lidar. Sensors 17 (10), 2371. http://dx.doi.org/10.3390/s17102371.

Bremer, M., Wichmann, V., Rutzinger, M., 2017. Calibration and validation of a detailed architectural canopy model reconstruction for the simulation of synthetic hemispherical images and airborne lidar data. Remote Sens. 9 (3), 220. http://dx.doi.org/10.3390/rs9030220.

Bremer, M., Wichmann, V., Rutzinger, M., 2018. Multi-temporal fine-scale modelling of larix decidua forest plots using terrestrial lidar and hemispherical photographs. Remote Sens. Environ. 206, 189–204. http://dx.doi.org/10.1016/j.rse.2017.12.023.

Bruggisser, M., Hollaus, M., Kükenbrink, D., Pfeifer, N., 2019. Comparison of forest structure metrics derived from uav lidar and als data. ISPRS Ann. Photogramm. Remote Sens. Spat. Inf. Sci. IV-2/W5, 325–332. http://dx.doi.org/10.5194/isprs-annals-IV-2-W5-325-2019.

Calders, K., Newnham, G., Burt, A., Murphy, S., Raumonen, P., Herold, M., Culvenor, D., Avitabile, V., Disney, M., Armston, J., et al., 2015. Nondestructive estimates of above-ground biomass using terrestrial laser scanning. Methods Ecol. Evol. 6 (2), 198–208. http://dx.doi.org/10.1111/2041-210X.12301.

Calders, K., Origo, N., Burt, A., Disney, M., Nightingale, J., Raumonen, P., Åkerblom, M., Malhi, Y., Lewis, P., 2018. Realistic forest stand reconstruction from terrestrial lidar for radiative transfer modelling. Remote Sens. 10 (6), 933. http://dx.doi.org/10.3390/rs10060933.

Côté, J.-F., Fournier, R.A., Egli, R., 2011. An architectural model of trees to estimate forest structural attributes using terrestrial lidar. Environ. Model. Softw. 26 (6), 761–777. http://dx.doi.org/10.1016/j.envsoft.2010.12.008.

Côté, J.-F., Widlowski, J.-L., Fournier, R.A., Verstraete, M.M., 2009. The structural and radiative consistency of three-dimensional tree reconstructions from terrestrial lidar. Remote Sens. Environ. 113 (5), 1067–1081. http://dx.doi.org/10.1016/j.rse.2009.01.017.

Gaveau, D.L., Hill, R.A., 2003. Quantifying canopy height underestimation by laser pulse penetration in small-footprint airborne laser scanning data. Can. J. Remote Sens. 29 (5), 650–657. http://dx.doi.org/10.5589/m03-023.

Hackenberg, J., Wassenberg, M., Spiecker, H., Sun, D., 2015. Non destructive method for biomass prediction combining tls derived tree volume and wood density. Forests 6 (4), 1274–1300. http://dx.doi.org/10.3390/f6041274.

Heinzel, J., Huber, M.O., 2017. Detecting tree stems from volumetric tls data in forest environments with rich understory. Remote Sens. 9 (1), 9. http://dx.doi.org/10.3390/rs9010009.

Hopkinson, C., 2007. The influence of flying altitude, beam divergence, and pulse repetition frequency on laser pulse return intensity and canopy frequency distribution. Can. J. Remote Sens. 33 (4), 312–324. http://dx.doi.org/10.5589/m07-029.

Jaakkola, A., Hyyppä, J., Kukko, A., Yu, X., Kaartinen, H., Lehtomäki, M., Lin, Y., 2010. A low-cost multi-sensoral mobile mapping system and its feasibility for tree measurements. ISPRS J. Photogramm. Remote Sens. 65 (6), 514–522. http://dx.doi.org/10.1016/j.isprsjprs.2010.08.002.

Jenkins, J.C., Chojnacky, D.C., Heath, L.S., Birdsey, R.A., 2003. National-scale biomass estimators for united states tree species. Forest Sci. 49 (1), 12–35. http://dx.doi.org/10.1093/forestscience/49.1.12.

Kankare, V., Puttonen, E., Holopainen, M., Hyyppä, J., 2016. The effect of tls point cloud sampling on tree detection and diameter measurement accuracy. Remote Sens. Lett. 7 (5), 495–502. http://dx.doi.org/10.1080/2150704X.2016.1157639.

Keith, H., Barrett, D., Keenan, R., 2000. Review of Allometric Relationships for Estimating Woody Biomass for New South Wales, the Australian Capital Territory, Victoria, Tasmania and South Australia. Australian Greenhouse Office, Canberra, Australia.

Liang, X., Hyyppä, J., Kaartinen, H., Lehtomäki, M., Pyörälä, J., Pfeifer, N., Holopainen, M., Brolly, G., Francesco, P., Hackenberg, J., Huang, H., Jo, H.-W., Katoh, M., Liu, L., Mokroš, M., Morel, J., Olofsson, K., Poveda-Lopez, J., Trochta, J., Wang, D., Wang, J., Xi, Z., Yang, B., Zheng, G., Kankare, V., Luoma, V., Yu, X., Chen, L., Vastaranta, M., Saarinen, N., Wang, Y., 2018. International benchmarking of terrestrial laser scanning approaches for forest inventories. ISPRS J. Photogramm. Remote Sens. (ISSN: 0924-2716) 144, 137–179. http://dx.doi.org/10.1016/j.isprsjprs.2018.06.021.

Liang, X., Kankare, V., Hyyppä, J., Wang, Y., Kukko, A., Haggrén, H., Yu, X., Kaartinen, H., Jaakkola, A., Guan, F., Holopainen, M., Vastaranta, M., 2016. Terrestrial laser scanning in forest inventories. ISPRS J. Photogramm. Remote Sens. 115, 63–77. http://dx.doi.org/10.1016/j.isprsjprs.2016.01.006.

Liang, X., Kankare, V., Yu, X., Hyyppä, J., Holopainen, M., 2014. Automated stem curve measurement using terrestrial laser scanning. IEEE Trans. Geosci. Remote Sens. 52 (3), 1739–1748. http://dx.doi.org/10.1109/TGRS.2013.2253783.

Liang, X., Litkey, P., Hyyppa, J., Kaartinen, H., Vastaranta, M., Holopainen, M., 2012. Automatic stem mapping using single-scan terrestrial laser scanning. IEEE Trans. Geosci. Remote Sens. 50 (2), 661–670. http://dx.doi.org/10.1109/TGRS.2011.2161613.

Liang, X., Wang, Y., Pyörälä, J., Lehtomäki, M., Yu, X., Kaartinen, H., Kukko, A., Honkavaara, E., Issaoui, A.E., Nevalainen, O., Vaaja, M., Virtanen, J.-P., Katoh, M., Deng, S., 2019. Forest in situ observations using unmanned aerial vehicle as an alternative of terrestrial measurements. Forest Ecosyst. 6 (1), 20. http://dx.doi.org/10.1186/s40663-019-0173-3.

Lindberg, E., Holmgren, J., Olofsson, K., Olsson, H., 2012. Estimation of stem attributes using a combination of terrestrial and airborne laser scanning. Eur. J. Forest Res. 131 (6), 1917–1931. http://dx.doi.org/10.1007/s10342-012-0642-5.

Maas, H.-G., Bienert, A., Scheller, S., Keane, E., 2008. Automatic forest inventory parameter determination from terrestrial laser scanner data. Int. J. Remote Sens. 29 (5), 1579–1593. http://dx.doi.org/10.1080/01431160701736406.

Mandlburger, G., Hollaus, M., Glira, P., Wieser, M., Milenković, M., 2015. First examples from the riegl vux-sys for forestry applications. In: Proceedings of SilviLaser. 28-30 September 2015, La Grande Motte, France. pp. 105–107.

McRoberts, R.E., Tomppo, E.O., 2007. Remote sensing support for national forest inventories. Remote Sens. Environ. 110 (4), 412–419. http://dx.doi.org/10.1016/j.rse.2006.09.034.

Morsdorf, F., Eck, C., Zgraggen, C., Imbach, B., Schneider, F.D., Kükenbrink, D., 2017. UAV-based LiDAR acquisition for the derivation of high-resolution forest and ground information. Lead. Edge 36 (7), 566–570.

Morsdorf, F., Frey, O., Meier, E., Itten, K.I., Allgöwer, B., 2008. Assessment of the influence of flying altitude and scan angle on biophysical vegetation products derived from airborne laser scanning. Int. J. Remote Sens. 29 (5), 1387–1406. http://dx.doi.org/10.1080/01431160701736349.

Morsdorf, F., Kükenbrink, D., Schneider, F., Abegg, M., Schaepman, M., 2018. Close-range laser scanning in forests: Towards physically based semantics across scales. Interface Focus 8 (2), 20170046. http://dx.doi.org/10.1098/rsfs.2017.0046.

Muukkonen, P., 2006. Forest inventory-based large-scale forest biomass and carbon budget assessment: new enhanced methods and use of remote sensing for verification. Dissertationes For. 30.

Næsset, E., 2009. Effects of different sensors, flying altitudes, and pulse repetition frequencies on forest canopy metrics and biophysical stand properties derived from small-footprint airborne laser data. Remote Sens. Environ. 113 (1), 148–159. http://dx.doi.org/10.1016/j.rse.2008.09.001.

Olofsson, K., Holmgren, J., Olsson, H., 2014. Tree stem and height measurements using terrestrial laser scanning and the ransac algorithm. Remote Sens. 6 (5), 4323–4344. http://dx.doi.org/10.3390/rs6054323.

Pfeifer, N., Mandlburger, G., 2017. Lidar data filtering and dtm generation. In: Topographic Laser Ranging and Scanning. CRC Press, pp. 307–334.

Pfeifer, N., Mandlburger, G., Otepka, J., Karel, W., 2014. Opals–a framework for airborne laser scanning data analysis. Comput. Environ. Urban Syst. 45, 125–136. http://dx.doi.org/10.1016/j.compenvurbsys.2013.11.002.

Pfeifer, N., Winterhalder, D., 2004. Modelling of tree cross sections from terrestrial laser scanning data with free-form curves. Int. Arch. Photogramm. Remote Sens. Spat. Inf. Sci. 36, 76–81.

Piermattei, L., Karel, W., Wang, D., Wieser, M., Mokroš, M., Surovỳ, P., Koreň, M., Tomaštík, J., Pfeifer, N., Hollaus, M., 2019. Terrestrial structure from motion photogrammetry for deriving forest inventory data. Remote Sens. 11 (8), 950. http://dx.doi.org/10.3390/rs11080950.

Puttonen, E., Lehtomäki, M., Kaartinen, H., Zhu, L., Kukko, A., Jaakkola, A., 2013. Improved sampling for terrestrial and mobile laser scanner point cloud data. Remote Sens. 5 (4), 1754–1773. http://dx.doi.org/10.3390/rs5041754.

Raumonen, P., Kaasalainen, M., Åkerblom, M., Kaasalainen, S., Kaartinen, H., Vastaranta, M., Holopainen, M., Disney, M., Lewis, P., 2013. Fast automatic precision tree models from terrestrial laser scanner data. Remote Sens. 5 (2), 491–520.

Saarinen, N., Kankare, V., Vastaranta, M., Luoma, V., Pyörälä, J., Tanhuanpää, T., Liang, X., Kaartinen, H., Kukko, A., Jaakkola, A., et al., 2017. Feasibility of terrestrial laser scanning for collecting stem volume information from single trees. ISPRS J. Photogramm. Remote Sens. 123, 140–158.

Schneider, F.D., Kükenbrink, D., Schaepman, M.E., Schimel, D.S., Morsdorf, F., 2019. Quantifying 3d structure and occlusion in dense tropical and temperate forests using close-range lidar. Agric. Forest Meteorol. 268, 249–257. http://dx.doi.org/10.1016/j.agrformet.2019.01.033.

Thies, M., Pfeifer, N., Winterhalder, D., Gorte, B.G., 2004. Three-dimensional reconstruction of stems for assessment of taper, sweep and lean based on laser scanning of standing trees. Scand. J. Forest Res. 19 (6), 571–581. http://dx.doi.org/10.1080/02827580410019562.

Van Leeuwen, M., Hilker, T., Coops, N.C., Frazer, G., Wulder, M.A., Newnham, G.J., Culvenor, D.S., 2011. Assessment of standing wood and fiber quality using ground and airborne laser scanning: a review. Forest Ecol. Manag. 261 (9), 1467–1478. http://dx.doi.org/10.1016/j.foreco.2011.01.032.

Vauhkonen, J., Rombouts, J., Maltamo, 2014. Inventory of forest plantations. In: Maltamo, M., Næsset, E., Vauhkonen, J. (Eds.), Forestry Applications of Airborne Laser Scanning: Concepts and Case Studies. In: Managing Forest Ecosystems, vol. 27, Springer, The Netherlands, pp. 253–268, 464pp.

Wallace, L., Lucieer, A., Watson, C., Turner, D., 2012. Development of a uav-lidar system with application to forest inventory. Remote Sens. 4 (6), 1519–1543. http://dx.doi.org/10.3390/rs4061519.

Wallace, L., Musk, R., Lucieer, A., 2014. An assessment of the repeatability of automatic forest inventory metrics derived from UAV-borne laser scanning data. IEEE Trans. Geosci. Remote Sens. 52 (11), 7160–7169. http://dx.doi.org/10.1109/TGRS.2014.2308208.

Wang, D., Hollaus, M., Puttonen, E., Pfeifer, N., 2016a. Automatic and self-adaptive stem reconstruction in landslide-affected forests. Remote Sens. 8 (12), 974. http://dx.doi.org/10.3390/rs8120974.

Wang, D., Hollaus, M., Puttonen, E., Pfeifer, N., 2016b. Fast and robust stem reconstruction in complex environments using terrestrial laser scanning. Int. Arch. Photogramm. Remote Sens. Spat. Inf. Sci. 41, http://dx.doi.org/10.5194/isprs-archives-xli-b3-411-2016.

Wang, D., Kankare, V., Puttonen, E., Hollaus, M., Pfeifer, N., 2017. Reconstructing stem cross section shapes from terrestrial laser scanning. IEEE Geosci. Remote Sens. Lett. (ISSN: 1545-598X) 14 (2), 272–276. http://dx.doi.org/10.1109/LGRS.2016.2638738.

Wang, D., Momo Takoudjou, S., Casella, E., 2019. Lewos: A universal leaf-wood classification method to facilitate the 3d modelling of large tropical trees using terrestrial lidar. Methods Ecol. Evol. http://dx.doi.org/10.1111/2041-210X.13342.

Wieser, M., Hollaus, M., Mandlburger, G., Glira, P., Pfeifer, N., 2016. ULS LiDAR supported analyses of laser beam penetration from different ALS systems into vegetation. ISPRS Ann. Photogramm. Remote Sens. Spat. Inf. Sci. III-3, 233–239. http://dx.doi.org/10.5194/isprsannals-III-3-233-2016.

Wieser, M., Mandlburger, G., Hollaus, M., Otepka, J., Glira, P., Pfeifer, N., 2017. A case study of uas borne laser scanning for measurement of tree stem diameter. Remote Sens. 9 (11), 1154. http://dx.doi.org/10.3390/rs9111154.

Wilkes, P., Lau, A., Disney, M., Calders, K., Burt, A., de Tanago, J.G., Bartholomeus, H., Brede, B., Herold, M., 2017. Data acquisition considerations for terrestrial laser scanning of forest plots. Remote Sens. Environ. 196, 140–153. http://dx.doi.org/10.1016/j.rse.2017.04.030.

Yu, X., Liang, X., Hyyppä, J., Kankare, V., Vastaranta, M., Holopainen, M., 2013. Stem biomass estimation based on stem reconstruction from terrestrial laser scanning point clouds. Remote Sens. Lett. 4 (4), 344–353. http://dx.doi.org/10.1080/2150704X.2012.734931.